

# Singularity and universality from von Neumann to Rényi entanglement entropy and disorder operator in Motzkin chains

Jianyu Wang,<sup>1, 2, 3, 4, 5</sup> Zenan Liu,<sup>6, 5</sup> Zheng Yan,<sup>6, 5, \*</sup> and Congjun Wu<sup>2, 3, 4, 5, †</sup>

<sup>1</sup>*State Key Laboratory of Surface Physics and Department of Physics, Fudan University, Shanghai 200438, China*

<sup>2</sup>*New Cornerstone Science Laboratory, Department of Physics,  
School of Science, Westlake University, Hangzhou 310024, China*

<sup>3</sup>*Institute for Theoretical Sciences, Westlake University, Hangzhou 310024, China*

<sup>4</sup>*Key Laboratory for Quantum Materials of Zhejiang Province,  
School of Science, Westlake University, Hangzhou 310024, China*

<sup>5</sup>*Institute of Natural Sciences, Westlake Institute for Advanced Study, Hangzhou 310024, China*

<sup>6</sup>*Department of Physics, School of Science and Research Center for  
Industries of the Future, Westlake University, Hangzhou 310030, China*

(Dated: February 18, 2025)

The Rényi entanglement entropy is widely used in studying quantum entanglement properties in strongly correlated systems, whose analytic continuation as the Rényi index  $n \rightarrow 1$  is often believed to yield the von Neumann entanglement entropy. However, earlier findings indicate that this process exhibits a singularity or the colored Motzkin spin chain problem, leading to different scaling behaviors of  $\sim \sqrt{l}$  and  $\sim \log l$  for the von Neumann and Rényi entropies, respectively. Our analytical and numerical calculations confirm this transition, which can be explained by the exponentially increasing density of states in the entanglement spectrum that we extract numerically. Disorder operators are further employed under various symmetries to study such a system. Both analytical and numerical results demonstrate that the scaling of the disorder operators also follows  $\log l$  as the leading behavior, matching that of the Rényi entropy. We propose that the coefficient of the term  $\log l$  is a universal constant shared by both the Rényi entropies and disorder operators. This universal constant could potentially help capture the underlying constraint physics of Motzkin walks.

## I. INTRODUCTION

In recent years, the interflow and mutual learning between condensed matter and quantum information have inspired increasingly fruitful research [1–3]. In the field of quantum information, the entanglement entropy (EE) plays a key role in measuring information and chaos [4, 5]. As one of the basic properties of quantum mechanics, quantum entanglement itself is difficult to measure. Moreover, the introduction of EE in condensed matter physics has revealed rich physics, such as topological entanglement entropy and long-range entanglement in highly entangled matter [6, 7]. One important topic in condensed matter physics is using EE to probe the intrinsic physics of many-body systems [6–10]. Among many intriguing features, EE offers a direct connection between the conformal field theory (CFT) and categorical description of the problems beyond traditional observables [11–27].

Unlike in few-body systems, the scaling behaviors of EE in quantum many-body systems reveal universal properties, such as the central charge [11, 28–30], number of Goldstone modes [31–34], and quantum dimension of topological order [6, 7, 24, 35]. Within the frame-

work of CFT [15, 36–39], the EE with cornered cuttings in two-dimensional quantum systems usually obeys the area-law  $s = al + bln l + \delta$ , where  $l$  is the length of the entangled boundary;  $b$  is related to the angles of corners;  $a$  is generally thought to be UV dependent. Meanwhile, the coefficients  $b$  and  $\delta$  usually can be employed to extract universal information, and detect novel phases and criticalities [2].

The von Neumann (VN) EE  $s_A^{\text{VN}} = -\text{Tr}(\rho_A \log \rho_A)$  ( $\rho_A$  is the reduced density matrix) as the generalization of the Shannon entropy in quantum mechanics is widely used in studying the above questions [40–43]. However, due to the difficulty in the calculation of the VN EE, the Rényi EE is much more commonly used both in field theory and numeric calculations. The definition of the Rényi EE is  $s_A^{(n)} = \frac{1}{1-n} \log [\text{Tr}(\rho_A^n)]$  with  $n$  the Rényi index. Formally, the Rényi EE becomes the VN EE as  $n \rightarrow 1$ . Although the Rényi EE loses certain properties including additivity and sub-additivity [44–48], it is strongly believed to yield the same scaling behaviors as the VN EE, such as the area and volume laws. It has been demonstrated in the past that all the coefficients of the VN EE for each  $O(l)$  term can be obtained via the analytic continuation of  $n$ . For a large number of examples including both field theoretical and numerical results, this common belief has been massively tested [49, 50].

However, the colored Motzkin spin chain was found as a counter example in previous studies [51–53]. There

\* zhengyan@westlake.edu.cn

† wucongjun@westlake.edu.cn

is a singularity in the limit of Rényi index  $n \rightarrow 1$ , in which the coefficient of the leading term  $\log l$  will be divergent. It actually indicates that an extra term  $\sqrt{l}$  becomes the leading term in the VN EE. This result provides a counter-example for the analytic continuation from Rényi to von Neumann EE, which cautions people should be careful in EE studies.

On the other hand, the disorder operator (DO) is a non-local observable, similar to the EE, which is proposed to extract the high-form symmetry and CFT information of quantum many-body systems [54–57]. It has been successfully used to detect the high-form symmetry breaking at the Ising transition [58]. The current central charges in CFT can be captured from the DO at phase transitions of the  $O(2)$  and  $O(3)$  universal classes in (2+1)D [59, 60]. DOs are also designed for fermionic systems to explore the universal feature of the Fermi liquid, Luttinger liquid, and quantum critical point (QCP) in fermionic systems [61–63]. The DO satisfies the universal scaling behaviors, where the logarithmic term usually reflects the general feature of CFT at a conformal invariant QCP.

In this article, we systematically study the scaling behaviors of VN and Rényi EE of a 1D colored Motzkin spin chain with different spin  $S$  both analytically and numerically. The scaling behaviors of DO for the Motzkin spin are also investigated, which are similar to the Rényi EE. Moreover, the coefficient of the logarithmic term is universal for any spin value, regardless of DO or EE.

The rest part of this paper is organized as follows. In Sec. II, the background of the Motzkin chain is presented. In Sec. III, the analytic solution of EE is given, encompassing an analysis of Rényi entanglement entropy to facilitate further discussions. In Sec. IV, we introduce the algorithm for Monte Carlo simulations and provide a detailed discussion of the numerical results for entanglement entropy. In Sec. V, we focus on the disorder operators of the Motzkin chain, exploring both analytical and numerical perspectives, and reveal that these disorder operators scale as  $\frac{3}{2} \log l$ . The summary and conclusion are presented in Sec. V.

## II. BACKGROUND OF MOTZKIN CHAINS

In this section, we review the concept of Motzkin chain, which is a 1D spin chain inspired by the Motzkin number [64, 65] from the combinatorial mathematics .

Motzkin walk or Motzkin path is a kind of non-negative lattice path defined as follows. Considering random walks starting from the point  $(0, 0)$  and ending at  $(2l, 0)$  on the  $x$ - $y$  plane as shown in Fig.1, they consist of three types of steps: upward steps  $\swarrow$ , downward steps  $\searrow$ , and horizontal steps  $\text{---}$ , represented as vectors  $(1, 1)$ ,  $(1, -1)$  and  $(1, 0)$ , respectively. Then Motzkin walks are random walks that do not cross below the  $x$ -axis ( $y = 0$ ). Bravyi et al. [66] introduced a frustrated-free spin-1 chain model whose unique ground state is the superposition of

all Motzkin walks states, achieved by mapping the spin  $S^z$  states  $\{\uparrow, 0, \downarrow\}$  to the steps  $\{\swarrow, \text{---}, \searrow\}$ , respectively. Movassagh and Shor [51] then generalized this model into an  $S$ -colored Motzkin model, where the upward or downward steps are colored using  $S$  different colors. This model can be translated to a spin- $S$  quantum chain. An example of the 2-colored Motzkin walk is shown in Fig. 1. For a 1D  $S$ -colored Motzkin model of size  $2l$ , the Hamiltonian is constructed by local projection operators with the following form:

$$H = \Pi^{\text{boundary}} + \sum_{j=1}^{2l-1} \Pi_{j,j+1}^{\text{cross}} + \sum_{j=1}^{2l-1} \Pi_{j,j+1}^{\text{exchange}}, \quad (1)$$

with

$$\begin{aligned} \Pi^{\text{boundary}} &= \sum_{k=1}^S \left( |\downarrow^k\rangle_{1,1} \langle \downarrow^k| + |\uparrow^k\rangle_{2l,2l} \langle \uparrow^k| \right), \\ \Pi_{j,j+1}^{\text{cross}} &= \sum_{k \neq k'}^S |\uparrow^k \downarrow^{k'}\rangle_{j,j+1} \langle \uparrow^k \downarrow^{k'}|, \\ \Pi_{j,j+1}^{\text{exchange}} &= \sum_{k=1}^S |D^k\rangle_{j,j+1} \langle D^k| + |U^k\rangle_{j,j+1} \langle U^k| \\ &\quad + |V^k\rangle_{j,j+1} \langle V^k|, \end{aligned} \quad (2)$$

where the superscript  $k$  indicate colors, *i.e.*,  $\uparrow^k$  stands for the  $S^z = k$  state and  $\downarrow^k$  stands for the  $S^z = -k$  state.

The boundary term ensures that the first and last steps do not pass below the  $x$ -axis. The cross term keeps the correct order of different color pairs. As a counter-example,  $\uparrow^k \uparrow^{k'} \downarrow^{k'} \downarrow^k$  is not allowed if  $k \neq k'$ . And the exchange term contains states  $|D^k\rangle = |\downarrow^k 0\rangle - |0 \downarrow^k\rangle$ ,  $|U^k\rangle = |\uparrow^k 0\rangle - |0 \uparrow^k\rangle$  and  $|V^k\rangle = |\uparrow^k \downarrow^k\rangle - |00\rangle$ , which leads to the steps exchanging of

$$\swarrow \leftrightarrow \text{---}, \quad \searrow \leftrightarrow \swarrow, \quad \text{---} \leftrightarrow \text{---}. \quad (3)$$

Notice that there is no such step exchange as

$$\swarrow \leftrightarrow \text{---}. \quad (4)$$

This property ensures that the walk height remains positive.

The ground state of the Hamiltonian (1) is the superposition of all the Motzkin walk configurations  $|M_i\rangle$  [66],

$$|G\rangle = \frac{1}{\sqrt{N}} \sum_i^N |M_i\rangle, \quad (5)$$

where  $N$  is the number of all the Motzkin walks allowed.

## III. THE VN AND RÉNYI EE'S

The entanglement between two subsystems by cutting the Motzkin chain at the midpoint is analytically studied in this section. It is worth noting that the similar

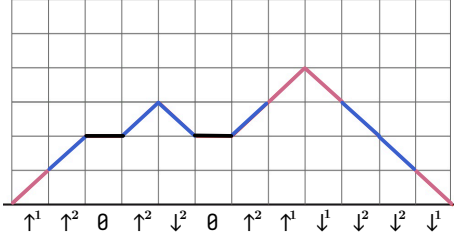


FIG. 1. Example of a 2-colored Motzkin walk (colored path). The walk starts and ends on the  $x$ -axis, and cannot cross below it. It can be mapped to a  $S^z$  configuration of a spin-2 chain. In this figure, the pink upward and downward steps are mapped to  $S^z = \pm 1$ , the blue steps are mapped to  $S^z = \pm 2$ , and the black horizontal steps are mapped to  $S^z = 0$ .

results have been studied in Refs. [51, 52], i.e., the VN EE and Rényi EE of colored Motzkin chain exhibit different scalings. In order for the article to be self-contained, we present the calculation of the Rényi EE here. Our analytical method is different from those in literature.

Consider a  $S$ -colored Motzkin chain with the size  $2l$ . The VN EE of the half-cutting takes the form as [51]

$$s^{\text{VN}} = a\sqrt{l} + b\log l + \text{const.}, \quad (6)$$

with

$$a = 2\sqrt{\frac{2\sqrt{S}}{(2\sqrt{S}+1)\pi}} \log S, \quad b = \frac{1}{2}. \quad (7)$$

The Rényi EE ( $n > 1$ ) is [52]

$$s^{(n)} = b\log l + \text{const.}, \quad (8)$$

with

$$b = \frac{3}{2} \left( 1 + \frac{1}{n-1} \right). \quad (9)$$

The VN and Rényi EE's exhibit different scaling behaviors. For comparison, when  $S = 1$  (colorless case) the leading terms of both the VN EE and Rényi EE are  $\frac{1}{2}\log l$ . As a notation, the “log” in this article stands for the natural logarithm.

For the completeness of the article and convenience of further analyses, we provide the derivation of the Rényi EE  $s^{(n)}$ . This analysis below elucidates the emergence of a singularity at  $n \rightarrow 1$ , whereby the VN EE and Rényi EE exhibit distinct scaling regimes governed by discontinuous analytic continuations.

### A. Analytical calculation of Rényi EE

Given the ground state wavefunction of Eq. (5), the eigenvalues of the reduced density matrix's of the half-chain are [51]

$$\lambda_m \simeq \frac{S^{-m}}{T} \frac{m^2}{l} \exp \left[ -\frac{1}{2}(2 + \frac{1}{\sqrt{S}}) \frac{m^2}{l} \right], \quad (10)$$

where the index  $m$  takes integer values from 0 to  $l$ , corresponding to the midpoint height of the Motzkin walk. The degeneracy of the eigenvalue  $\lambda_m$  is  $S^m$ , and  $\lambda_m$  reaches its maximum at an intermediate value of  $m$ . Additionally,  $T$  is a normalization factor that ensures  $\sum_m S^m \lambda_m = 1$ .

The  $n$ -th Rényi EE is then given by

$$\begin{aligned} s^{(n)} &= \frac{1}{1-n} \log \sum_{m=0}^l S^m \lambda_m^n \\ &= \frac{1}{1-n} \log \sum_{m=0}^l \frac{S^{(1-n)m}}{T} \frac{m^2}{l} \exp \left[ -\frac{1}{2}(2 + \frac{1}{\sqrt{S}}) \frac{m^2}{l} \right] \\ &= \frac{1}{1-n} \log \sum_{\xi=0}^{\sqrt{l}} \frac{S^{(1-n)\xi\sqrt{l}}}{T} \xi^2 \exp \left[ -\frac{1}{2}(2 + \frac{1}{\sqrt{S}}) \xi^2 \sqrt{l} \right], \end{aligned} \quad (11)$$

where we set  $\xi = m/\sqrt{l}$  in the last line.

Using the integral approximation to Eq. (11), the Rényi EE ( $n > 1$ ) is expressed as

$$\begin{aligned} s^{(n)} &\simeq \frac{1}{2} \log l + \frac{1}{1-n} \log \tilde{T}^{-n} \int_0^{\sqrt{l}} d\xi \xi^{2n} \times \\ &\quad \exp \left[ -\frac{n}{2}(2 + \frac{1}{\sqrt{S}}) \xi^2 - (n-1) \log S \sqrt{l} \xi \right], \end{aligned} \quad (12)$$

where

$$\tilde{T} = \frac{T}{\sqrt{l}} \simeq \int_0^{\sqrt{l}} d\xi \xi^2 \exp \left[ -\frac{1}{2}(2 + \frac{1}{\sqrt{S}}) \xi^2 \right]. \quad (13)$$

For the case  $n > 1$ , the Rényi EE can be simplified to

$$s^{(n)} = \frac{1}{2} \log l - \frac{n}{1-n} \log \tilde{T} + R, \quad (14)$$

where

$$\begin{aligned} R &= \frac{1}{1-n} \log \int_0^{\sqrt{l}} d\xi \xi^{2n} \exp \left[ -\frac{n}{2}(2 + \frac{1}{\sqrt{S}}) \xi^2 \right. \\ &\quad \left. - (n-1) \log (S) \sqrt{l} \xi \right]. \end{aligned} \quad (15)$$

For convenience, the following functions are defined:

- Define functions  $p_1$  and  $p_2$  as

$$\begin{aligned} p_1(n, S) &= \frac{n}{2}(2 + \frac{1}{\sqrt{S}}), \\ p_2(n, S) &= (n-1) \log S. \end{aligned} \quad (16)$$

- Define function  $f_\alpha$  as

$$f_\alpha(l) = l^{\alpha/2} \exp [-(p_1 + p_2)l]. \quad (17)$$

- Define function  $F_\alpha$  as

$$F_\alpha(p_1, p_2, l) =$$

$$\int_0^{\sqrt{l}} d\xi \xi^\alpha \exp \left[ -p_1(n, S) \xi^2 - p_2(n, S) \sqrt{l} \xi \right]. \quad (18)$$

Consequently,  $R$  in Eq. (15) is expressed as

$$R = \frac{1}{1-n} \log F_{2n}. \quad (19)$$

The positive function  $F_\alpha$  has the limit of  $\lim_{l \rightarrow \infty} F_\alpha \rightarrow 0$ . Additionally, for the condition that  $n, S > 1$  and sufficiently large  $l$ , the following limit can be proved

$$F_\alpha \simeq \frac{p_2 \sqrt{l}}{\alpha + 1} F_{\alpha+1}. \quad (20)$$

## B. The scaling form of Rényi EE

Now we analyze the scaling of Rényi EE in Eq. (14). The first term contributes a logarithmic scaling obviously. The second term contributes a constant because  $\tilde{T}$  has an upper bound in the limit  $l \rightarrow \infty$ , which is

$$\lim_{l \rightarrow \infty} \tilde{T} = \sqrt{\frac{\pi}{2}} \left( 2 + \frac{1}{\sqrt{S}} \right)^{-\frac{3}{2}}. \quad (21)$$

Then only the third term  $R$  is needed to be calculated.

We aim to demonstrate that there exists a finite limit for  $R$  divided by  $\log l$  as  $l \rightarrow \infty$ :

$$\lim_{l \rightarrow \infty} \frac{R}{\log(l)}. \quad (22)$$

Substituting Eqs. (17) and (18) into Eq. (22) and using the L'Hôpital's rule, we obtain:

$$\begin{aligned} \lim_{l \rightarrow \infty} \frac{R}{\log(l)} &= \frac{2n+1}{2n-2} \lim_{l \rightarrow \infty} \frac{p_2 \sqrt{l} F_{2n+1}}{p_2 \sqrt{l} F_{2n+1} + p_1 F_{2n+2}} \\ &= \frac{2n+1}{2n-2}, \end{aligned} \quad (23)$$

for which the relation of Eq. (20) is used. This indicates that the scaling of the  $R$  is given by

$$R = \frac{2n+1}{2n-2} \log l + C, \quad (24)$$

where  $C$  is a constant.  $C$  is evaluated as follows:

$$\lim_{l \rightarrow \infty} \left( R - \frac{2n+1}{2n-2} \log l \right) = \frac{1}{1-n} \lim_{l \rightarrow \infty} \log \left( l^{\frac{2n+1}{2}} F_{2n} \right). \quad (25)$$

According to Eq. (20), the limit of the term in the logarithm function is

$$\lim_{l \rightarrow \infty} l^{\frac{2n+1}{2}} F_{2n} = \frac{\Gamma(2n+1)}{p_2^{2n}} \lim_{l \rightarrow \infty} \sqrt{l} F_0 = \frac{\Gamma(2n+1)}{p_2^{2n+1}}, \quad (26)$$

where  $\Gamma$  is the gamma function. Then

$$C = \frac{1}{1-n} \log \left( \frac{\Gamma(2n+1)}{p_2^{2n+1}} \right). \quad (27)$$

In short, by substituting Eqs. (21), (23) and (26) into Eq. (15), the expression of Rényi EE (for  $n > 1$  and  $S > 1$ ) in the large  $l$  limit becomes [52]

$$s^{(n)} = \frac{3}{2} \left( 1 + \frac{1}{n-1} \right) \log l + \delta, \quad (28)$$

where the constant  $\delta$  is

$$\begin{aligned} \delta &= \frac{1}{(n-1)} \left( \frac{n}{2} \log \frac{\pi}{2} - \frac{3n}{2} \log \left( 2 + \frac{1}{\sqrt{S}} \right) - \right. \\ &\quad \left. \log \Gamma(2n+1) + (2n+1) \log ((n-1) \log S) \right). \end{aligned} \quad (29)$$

By comparing with the entanglement entropy of a CFT theory, we propose that the coefficient  $\frac{3}{2}$  in the logarithmic term of Rényi EE is universal, while the constant term  $\delta$  is complex and non-universal.

## IV. NUMERICAL RESULT OF EE

Quantum Monte Carlo (MC) simulations have been widely used in calculating Rényi EE in quantum many-body systems in recent years [34, 67–77]. In this section, we use the MC method to estimate the scaling behaviors of VN EE and Rényi EE in the Motzkin chain.

Our simulation is based on the Swap operator method. For pure states that can be written as the product states of two subsystems  $A$  and  $B$ , the Swap $_A$  operator is defined as

$$\begin{aligned} \text{Swap}_A &\left( |A_1\rangle \otimes |B_1\rangle \right) \left( |A_2\rangle \otimes |B_2\rangle \right) \\ &= \left( |A_2\rangle \otimes |B_1\rangle \right) \left( |A_1\rangle \otimes |B_2\rangle \right). \end{aligned} \quad (30)$$

The ground state expectation value of the Swap $_A$  operator is the 2nd order Rényi EE [67, 72, 78],

$$s_A^{(2)} = -\log \text{Tr}(\rho_A^2) = -\log \langle \text{Swap}_A \rangle, \quad (31)$$

where  $\langle \dots \rangle$  indicates the expectation value with respect to the replica ground state,

$$|G\rangle^2 \equiv |G\rangle \otimes |G\rangle. \quad (32)$$

Based on properties of the ground states of colored Motzkin chain, our algorithm can be simplified, and then its accuracy significantly improved. The details of the algorithm are provided below.

### A. The Monte Carlo algorithm

The MC algorithm used to estimate the EE is presented below. The ground state given in Eq. (5) is positive-definite, hence, the expectation value of the Swap $_A$  operator in Eq. (31) can be written as

$$\langle \text{Swap}_A \rangle = \sum_{i_1, i_2} \frac{1}{N} \langle G |^2 \text{Swap}_A |M_{i_1}\rangle \otimes |M_{i_2}\rangle. \quad (33)$$

Based on this formula, it is straightforward to setup a MC algorithm to calculate the 2nd order Rényi EE  $s^{(2)}$ . One can simulate two replicas of configurations  $M_{i_1}$  and  $M_{i_2}$  with equal weights and measure the value of the estimator

$$\langle G \rangle^2 \text{Swap} |M_{i_1}\rangle \otimes |M_{i_2}\rangle. \quad (34)$$

However, the symmetries of the colored Motzkin chain ground state allow us to further simplify the algorithm, so that only one replica is needed to sample. In this work, we consider the Motzkin chain of the size  $2l$ , and study the entanglement of the subsystem by cutting at the midpoint. The length of the subsystem  $A$  is constrained to  $l$  in all the discussions below.

The swappability of Motzkin walks can be defined as follows. Exchanging half of the path of walks  $M_1$  and  $M_2$  generates two new walks denoted as  $\tilde{M}_1$  and  $\tilde{M}_2$ . We assert that  $M_1$  is swappable to  $M_2$  if  $\tilde{M}_1$  also qualifies as a Motzkin walk. It is easy to identify the following properties of the Motzkin walks swappability: (1) If  $M_1$  is swappable with  $M_2$ , then  $M_2$  is also swappable with  $M_1$ ; (2) If  $M_1$  is swappable with  $M_2$ , and  $M_2$  is swappable with  $M_3$ , it follows that  $M_1$  is swappable with  $M_3$ . Consequently, we can conclude that the measurement variable in Eq. (34) has only two possible values: It takes the value of one if  $M_{i_1}$  and  $M_{i_2}$  are swappable; otherwise, it takes the value of zero.

The colored Motzkin walks can then be categorized into classes  $c_m$  based on their swappability – walks within each class  $c_m$  are swappable with each other. In this context,  $m$  represents the height at the midpoint, which corresponds to the number of unpaired steps in half of the Motzkin walks. Notably, there are  $S^m$  equivalent classes, where the only distinction is the color permutation of the unpaired steps. Therefore, we define the superclasses  $C_m$ , which contain the  $S^m$  equivalent classes  $c_m$ . The relationship between the size of the superclass  $C_m$  represented as  $N_m$ , and the size of the class  $c_m$  represented as  $n_m$ , can be succinctly expressed by  $N_m = S^m n_m$ . With this understanding, we can simulate the distribution of  $C_m$ . The expectation value  $\langle \text{Swap}_l \rangle$  can be estimated using the frequency  $\Lambda_m$  of each superclass  $C_m$ . The 2nd order Rényi EE is given by the formula:

$$s^{(2)} = -\log \sum_m S^{-m} \Lambda_m^2. \quad (35)$$

To calculate Rényi EE of other Rényi index, we generalize the Swap operator and  $n$  replicas need to be sampled. However, our algorithm can be directly generalized to simulate the Rényi EE of any Rényi index  $n$ , where  $n$  could be any positive real number and is not constrained to be an integer, using the following formula:

$$s^{(n)} = \frac{1}{1-n} \log \sum_{m=0}^l S^{-m(n-1)} \Lambda_m^n. \quad (36)$$

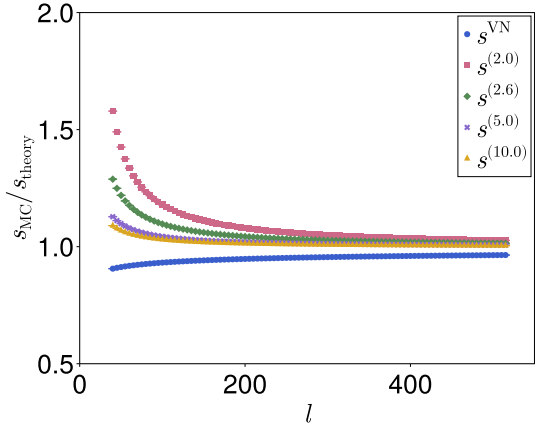


FIG. 2. The ratio of the EE results based on MC simulations and analytical calculations. The MC are simulated on a two-color ( $S = 2$ ) Motzkin chain of size  $2l$ , and the EE are calculated on the subsystem by cutting at the midpoint. As the subsystem size  $l$  increases, the ratio tends to be one, showing that the numerical and analytical results agree well for large system sizes.

Additionally, this algorithm can be employed to determine the VN EE, which is given by:

$$s^{\text{VN}} = - \sum_{m=0}^l S^{-m(n-1)} \Lambda_m \log \Lambda_m. \quad (37)$$

## B. Results of the EE from MC

The VN EE and Rényi EE computed by MC are presented in this subsection. Fig. (2) shows the comparison of our numerical results and the analytical results, demonstrating a good agreement. The ratios converge to 1 as increasing the system size.

The MC data of the Motzkin chain are analyzed through a fitting process. We fit the data using the form  $a\sqrt{l} + b\log l + \delta$ , where  $a$  could be zero. Here,  $l$  represents the size of the subsystem, which is determined by making a cut at the midpoint of the chain with length  $2l$ . The results of  $a$  are presented in Fig. (3). For the VN EE, indicated by the point at  $n = 1$ , the numerical results closely align with the analytical predictions. Furthermore, our findings indicate that the square root term tends to diminish as  $n$  increases, consistent with the previous analysis that the Rényi EE does not include a  $\sqrt{l}$  term. Fig. (4) presents the results of  $b$  and  $\delta$ , agreeing with analytical calculations.

We observe that there is an EE singularity of the Rényi index at  $n = 1$ , as indicated by both analytical and numerical results. The transition from a  $\log l$ -scaling to a  $\sqrt{l}$ -scaling is governed by the second term in the expansion of the Rényi entanglement entropy, as outlined in

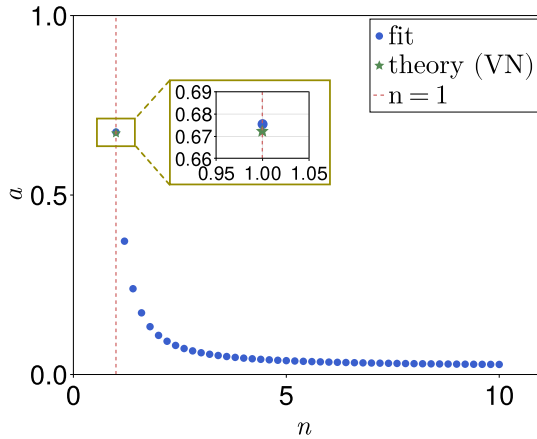


FIG. 3. The value of the coefficient of the  $\sqrt{l}$  term  $a$  in EE for a 2-colored ( $S = 2$ ) Motzkin chain. The fitting results are illustrated as blue dots, which are fitted with the form:  $a\sqrt{l} + b\log l + \delta$ , where  $l$  is the subsystem size. The theory prediction for VN EE is also shown as a green star. The MC are sampled on system size from 80 to 1230 sites.

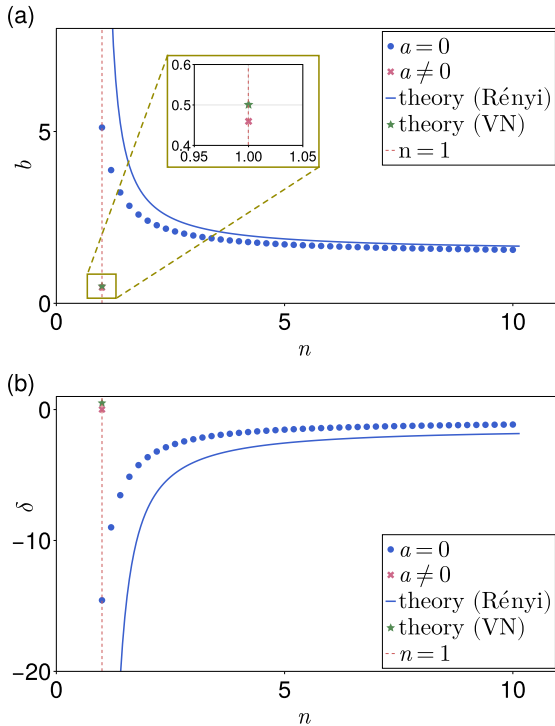


FIG. 4. The coefficient values in the scaling form of Rényi and VN EE for the 2-colored Motzkin chain. The MC are sampled on the system sizes from 80 to 1230 sites for the both two figures. The EE data are fitted by the form  $b\log l + \delta$ , represented by the blue dots. VN EE data are fitted by the form  $a\sqrt{l} + b\log l + \delta$ , represented by the pink crosses. The analytical results are also shown, respectively. (a) Value of  $b$ , the coefficient of the  $\log l$  term. (b) The constant term  $\delta$ .

Eq. (12):

$$\begin{aligned} & \frac{1}{1-n} \log F_{2n}(p_1, p_2) \tilde{T}^{-n} \\ &= \frac{1}{1-n} \log F_{2n}(p_1, p_2) F_2^{-n}(p_1, 0). \end{aligned} \quad (38)$$

The exact value of  $F_{2n}(p_1, p_2) F_2^{-n}(p_1, 0)$  can be determined in specific values of  $n$  and  $S$ . For the colorless Motzkin chain,  $p_2 = 0$ . It can be proved that  $F_{2n}(p_1, p_2) F_2^{-n}(p_1, 0) > 1$  and has an upper bound in the large  $l$  limit, thus Eq. (38) contributes a constant term to the scaling of EE. For the case  $S > 1$ , however, the value of  $F_{2n}(p_1, p_2) F_2^{-n}(p_1, 0)$  can be determined in specific values of  $(n-1)\sqrt{l}$  in the large  $l$  limit. It can be summarized as

$$F_{2n} \tilde{T}^{-n} = \begin{cases} 0, & (n-1)\sqrt{l} \rightarrow +\infty \\ 1, & (n-1)\sqrt{l} \rightarrow 0^+ \end{cases} \quad (39)$$

When analyzing the scaling of the Rényi EE, we will consider the limit  $(n-1)\sqrt{l} \rightarrow \infty$ . However, this term is treated as zero for the VN EE case. It reflects that the limits of  $l \rightarrow \infty$  and  $n \rightarrow 1$  do not commute in the EE calculation.

As  $n = 1$  (the VN EE) is the EE singularity of an infinite Motzkin spin chain, the finite-size modification becomes significantly large near  $n = 1$ . This finite-size effect is dominated by the term  $\frac{1}{(n-1)\sqrt{l}}$ , which accounts for the considerable difference observed between the analytical results and the numerical results shown in Fig. (4) as  $n$  approaches one.

From the perspective of the entanglement spectrum, the different scaling behavior of the von Neumann (VN) entanglement entropy (EE) from the Rényi EE arises from the abundance of high excited levels. Entanglement entropies can be understood as thermal entropies of an entanglement Hamiltonian  $H_E$ . The entanglement spectrum is of the eigenvalues of the entanglement Hamiltonian [79–81]. For any given Rényi index, the Rényi EE exhibits the same scaling and is solely dependent on the lower levels in the spectrum. In contrast, the exponentially large numbers of high excited levels — as shown in Fig. (5) — cause the VN EE to demonstrate a larger scaling behavior than the Rényi EE.

## V. DISORDER OPERATOR

The disorder operator [82–91] is a non-local operator capable of detecting higher-form symmetries, which are often challenging to measure by using local operators. For a system with global symmetry, the DO is defined as the symmetry operator that acts on a specific subsystem. Recent research [92–97] has demonstrated that the DO exhibits universal scaling behavior in various quantum systems. Typically, the scaling behavior of the minus

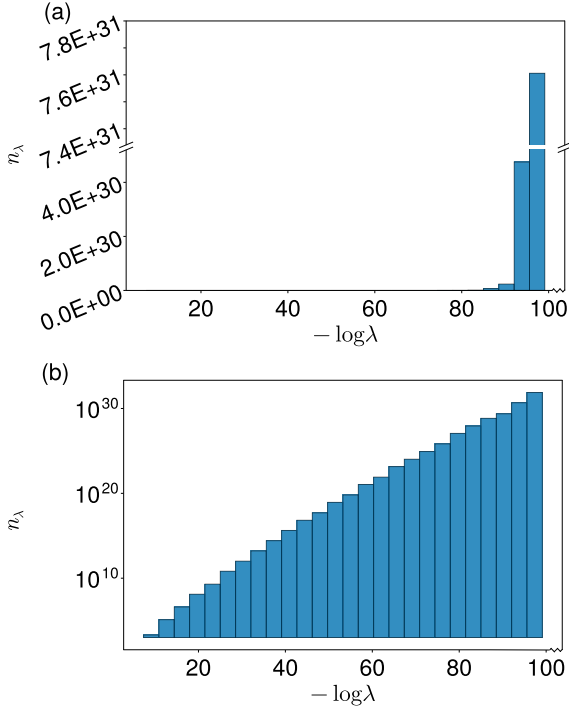


FIG. 5. The density of states in the entanglement spectrum, obtained by the reduced density matrix of a spin-2 chain of length 1070. The horizontal axis  $-\log \lambda$  is the eigenvalue of the entanglement Hamiltonian ( $\lambda$  is the eigenvalue of the reduced density matrix); the vertical axis is the density of states in a small window of  $-\log \lambda$  (using a natural or logarithmic scale in figures (a) and (b)).

of logarithm of DO is similar to the scaling behavior of entanglement entropy, which captures the essential information from CFT.

The Hamiltonian and the ground state of the colored Motzkin chain possess multiple symmetries [53]. Firstly, the colored Motzkin chain has the continuous  $U(1)$  symmetry characterized by the charge  $Q^z = \sum_j^{2l} S_j^z$ , where  $2l$  is the system size. Consequently, we define the DO as

$$X^z(\theta) = \prod_j^l e^{i\theta S_j^z}, \quad (40)$$

which acts solely on half of the chain obtained by cutting at the midpoint. The average of DO is then given by

$$\langle X^z(\theta) \rangle = \sum_{m=0}^l \lambda_m \left( \sum_{k=1}^S e^{ik\theta} \right)^m. \quad (41)$$

By substituting Eq. (10) into Eq. (41), setting  $\xi = \frac{m}{\sqrt{l}}$ , and utilizing the integral approximation, we arrive at the

following expression of DO:

$$\langle X^z(\theta) \rangle = \frac{1}{\sqrt{l}\tilde{T}} \int_0^\infty d\xi \sqrt{l}\xi^2 e^{-p_1(1,S)\xi^2} \times \left[ \frac{\sin(\frac{S\theta}{2})}{S \sin \frac{\theta}{2}} \right]^{\sqrt{l}\xi} e^{-i\frac{S+1}{2}\theta\sqrt{l}\xi}, \quad (42)$$

where  $\tilde{T}$  is defined in Eq. (21).

Define the following functions:

$$\chi_\alpha(S, \theta, l) = \int_0^\infty d\xi \xi^\alpha e^{-p_1(1,S)\xi^2} \left[ \frac{\sin(\frac{S\theta}{2})}{S \sin \frac{\theta}{2}} \right]^{\sqrt{l}\xi} e^{i\frac{S+1}{2}\theta\sqrt{l}\xi}, \quad (43)$$

$$y(S, \theta) = \log \left[ \frac{\sin(\frac{S\theta}{2})}{S \sin \frac{\theta}{2}} \right] + i\frac{S+1}{2}\theta. \quad (44)$$

Then the DO can be expressed as  $\langle X^z(\theta) \rangle = \chi_2$ . It is easy to prove the following relations:

$$\frac{d}{dl} \chi_\alpha = \frac{1}{2\sqrt{l}} y \chi_{\alpha+1}, \quad (45)$$

$$\chi_\alpha = -\frac{\sqrt{l}}{\alpha+1} y \chi_{\alpha+1} + 2p_1(1, S) \chi_{\alpha+2}. \quad (46)$$

Based on Eq. (45), we have

$$\chi_{\alpha+2} = \frac{2}{y^2} \frac{d}{dl} \chi_\alpha + \frac{4l}{y^2} \frac{d^2}{dl^2} \chi_\alpha. \quad (47)$$

Substituting it into Eq. (46), it yields

$$\chi_\alpha = \left( 2p_1 \frac{2}{y^2} - \frac{2l}{\alpha+1} \right) \frac{d}{dl} \chi_\alpha + \frac{8p_1}{y^2} l \frac{d^2}{dl^2} \chi_\alpha. \quad (48)$$

Now look at Eq. (46). There are two possibilities for the large  $l$  scaling of  $\chi_\alpha$ :

- $\chi_\alpha$  and  $\sqrt{l}\chi_{\alpha+1}$  have the same scaling order, while  $\chi_{\alpha+2}$  is at a smaller order of  $l$ ;
- $\sqrt{l}\chi_{\alpha+1}$  and  $\chi_{\alpha+2}$  have the same scaling order, while  $\chi_n$  is at a smaller order of  $l$ .

Other cases are impossible, which can be seen by writing down the recurrence relation of  $\chi_{\alpha+1}$ ,  $\chi_{\alpha+2}$  and  $\chi_{\alpha+3}$ . Then we have the following arguments about the two cases.

For the first case,  $\chi_{\alpha+1} \sim \chi_\alpha / \sqrt{l}$ . Substitute it into Eq.(45) and we have

$$\frac{d}{dl} \chi_\alpha \sim \frac{y}{l} \chi_\alpha. \quad (49)$$

Thus we can suppose that the scaling form of  $\chi_\alpha$  is

$$\chi_\alpha \sim l^\lambda, \quad (50)$$

and the value of  $\lambda$  can be determined by substituting Eq. (50) into Eq. (48):

$$l^\lambda = -\frac{2\lambda}{\alpha+1}l^\lambda + \frac{8p_1}{y^2}\lambda(\lambda+1)l^{\lambda-1}, \quad (51)$$

which yields  $\lambda = -(\alpha+1)/2$ . Thus, the scaling form of  $\chi_\alpha$  is  $\chi_\alpha \sim l^{-\frac{\alpha+1}{2}}$ .

For the second case,  $\chi_{\alpha+1} \sim \sqrt{l}\chi_\alpha$ . Substitute it into Eq.(45) and we have

$$\frac{d}{dl}\chi_\alpha \sim y\chi_\alpha. \quad (52)$$

So we can suppose that the leading term of the scaling form of  $\chi_\alpha$  is

$$\chi_\alpha \sim e^{\beta l}l^\lambda. \quad (53)$$

The value of  $\beta$  and  $\lambda$  can be determined by substituting Eq. (53) into Eq. (48)

$$\begin{aligned} l^\lambda &= \left( -\frac{2}{\alpha+1}\beta + \frac{8p_1}{y^2}\beta^2 \right) l^{\lambda+1} \\ &+ \left( \frac{4p_1}{y^2}\beta - \frac{2\lambda}{\alpha+1} + \frac{16p_1}{y^2}\beta\lambda \right) l^\lambda, \end{aligned} \quad (54)$$

which yields

$$\begin{aligned} \beta &= \frac{y^2}{4p_1(\alpha+1)} \\ \lambda &= \frac{\alpha}{2}. \end{aligned} \quad (55)$$

Thus we have  $\chi_\alpha \sim e^{\frac{y^2}{4p_1(\alpha+1)}l}\lambda^{\frac{\alpha}{2}}$ .

It is noteworthy that the term  $e^{-p_1(1,S)\xi^2}$  significantly suppresses the contribution from large  $\xi$  in the integral given in Eq. (43). Moreover, since  $\xi^\alpha$  is larger than  $\xi^{\alpha+1}$  for small  $\xi$ , we argue that  $\chi_\alpha$  has a larger scaling order in  $l$  than  $\chi_{\alpha+1}$ . This supports the validity of the first case in our situation. Additionally, Numerical calculation of Eq.(43) and MC results in the following also confirm the first case. We calculate the limit  $l \rightarrow \infty$  using Eq. (45) and (46),

$$\begin{aligned} \lim_{l \rightarrow \infty} \frac{-\log |\langle X^z(\theta) \rangle|}{\log l} &= -\lim_{l \rightarrow \infty} \frac{l \frac{d}{dl}\chi_2}{\chi_2} \\ &= \lim_{l \rightarrow \infty} \frac{-l \frac{1}{2\sqrt{l}}y\chi_3}{-\frac{\sqrt{l}}{3}y\chi_3 + 2p_1(1,S)\chi_4} = \frac{3}{2}. \end{aligned} \quad (56)$$

Therefore the scaling behavior of the minus of the logarithm of DO is expressed as:

$$-\log |\langle X^z(\theta) \rangle| = \frac{3}{2} \log l + \text{const.} \quad (57)$$

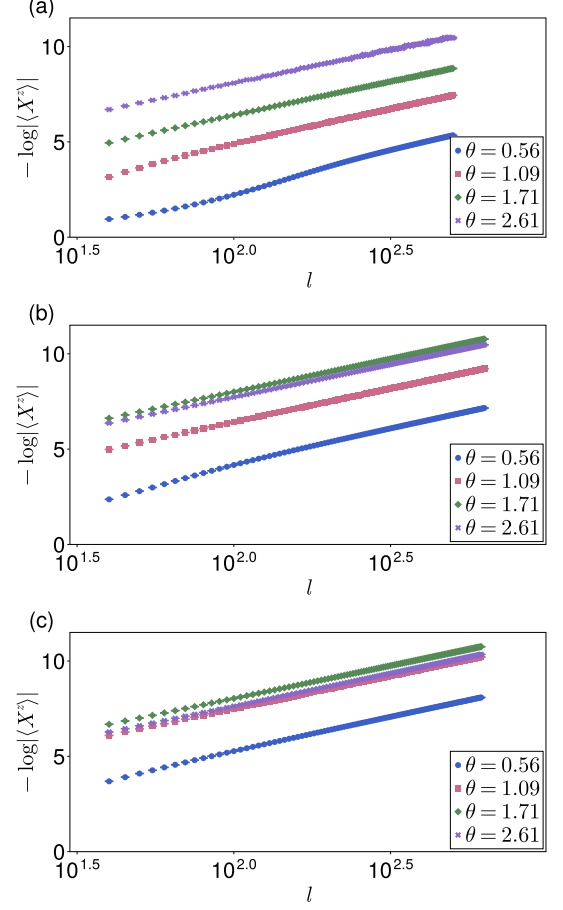


FIG. 6. The minus of logarithmic DO under  $U(1)$  symmetry with charge  $Q^z$ . The system is a 2-colored Motzkin chain with size  $2l$ , and the MC are sampled on system size ranging from 80 to 1230 sites. The horizontal axis is the subsystem size  $l$ , by cutting at the midpoint of the chain. (a) Colorless Motzkin chain. (b) 2-colored Motzkin chain. (c) 3-colored Motzkin chain.

Note that the result holds for both colorless and colored cases. The universal coefficient of the log term is  $\frac{3}{2}$ , the same as in the Rényi EE.

We calculate the DO numerically by using MC simulations, and the results of the cases of  $S = 1, 2, 3$  are presented in Fig. (6). It shows that the logarithmic scaling agrees well with the analytic result in Eq. (57).

The results presented in Eq. (57) hold true in the large  $l$  limit. Since  $l$  is always paired with  $\theta$  in Eq. (43), there is a competition between small  $\theta$  values and large  $l$  values. This competition leads to significant finite-size effects in the region of small  $\theta$ . Our simulation also verifies this competition between  $\theta$  and  $l$ . The DOs are fitted using the function  $b \log l + \text{const.}$ , based on the data of various segments of system sizes. The results for  $b$  are depicted in Fig. (7). The figure indicates that for small  $\theta$  values, there is a notable difference between  $b$  and  $3/2$ . However, as the system size increases, this difference tends to

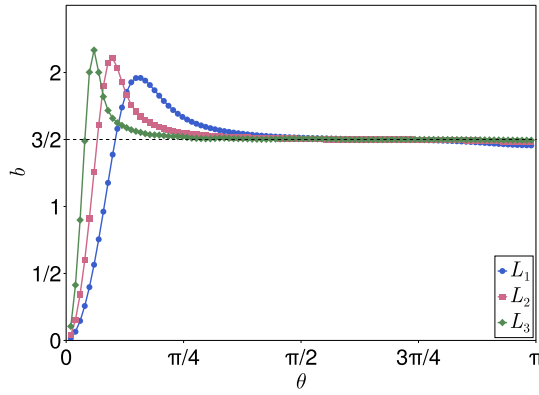


FIG. 7. The value of  $b$  by fitting the data of  $-\log |\langle X^z(\theta) \rangle|$  within the form  $b \log l + \text{const}$ . The horizontal axis represents the phase  $\theta$  in the  $U(1)$  symmetry. Different colors correspond to various system size segments. Specifically,  $L_1$  are system sizes ranging from 80 to 310 sites,  $L_2$  are from 300 to 530 sites and  $L_3$  are from 1020 to 1260 sites. The DOs are calculated on subsystems obtained by cutting at the chain at the midpoint. The value of  $b$  is approximately  $3/2$ , particularly in the large  $\theta$  region. The competition between  $\theta$  and  $l$  leads to a significant finite-size effect in the small  $\theta$  region. This finite-size effect diminishes as the system size  $l$  increases, as illustrated in the figure. Therefore, we argue that as the system size increases,  $b$  approaches  $3/2$  for any value of  $\theta$ , which aligns with our analytical predictions.

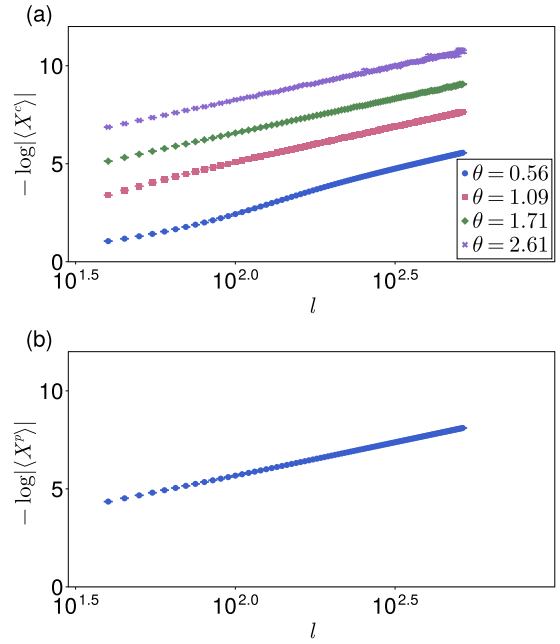


FIG. 8. The minus of the logarithms of DOs. The system is a 2-colored Motzkin chain, and the MC are sampled on system size ranging from 80 to 1230 sites. The horizontal axis is the subsystem size  $l$ , by cutting at the midpoint of the chain. (a) The DO of  $U(1)$  symmetry with charge  $Q^c$ . (b) The DO of permutation symmetry.

diminish.

In addition to the  $U(1)$  symmetry above, the ground state of the Motzkin chain exhibits an additional  $U(1)$  symmetry characterized by the charge  $Q^c = \sum_j^S \sum_k^l (|\uparrow^k\rangle_j \langle \uparrow^k| - |\downarrow^k\rangle_j \langle \downarrow^k|)$ . Then the associated DO is:

$$\begin{aligned} X^c(\theta) &= \left\langle \prod_j^l e^{\sum_k^S i\theta (|\uparrow^k\rangle_j \langle \uparrow^k| - |\downarrow^k\rangle_j \langle \downarrow^k|)} \right\rangle \\ &= \frac{1}{T} \sum_{m=0}^l \frac{m^2}{l} e^{-p_1(1,S) \frac{m^2}{l}} e^{ikm\theta}, \end{aligned} \quad (58)$$

Based on the similar calculation to  $X^z$ , in the limit of  $l \rightarrow \infty$ , the minus of logarithm of DO also has the  $\log l$  scaling behavior,

$$-\log |\langle X^c(\theta) \rangle| = \frac{3}{2} \log l + \text{const.} \quad (59)$$

The numerical results are illustrated in Fig. 8.(a).

The model has a permutation symmetry concerning different colors. Take the example in Fig.(1) for instance, it is still a Motzkin walk after exchanging the blue and pink steps. We introduce a DO of  $X^p$  that permutes colors within the subsystems. It can be proved that the

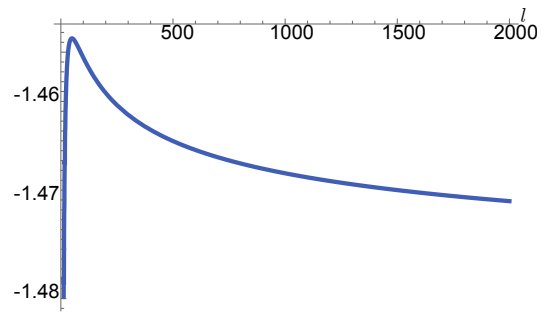


FIG. 9. The numerical results of the value of  $\log \left( (2\sqrt{S} + 1)^l \sum_{i=0}^{l/2} S^i \frac{l!}{(i+1)i!(l-2i)!} \right) / \log l$ . The horizontal axis is  $l$ . Based on this calculation results, we argue that as  $l \rightarrow \infty$ , the value goes to  $-1.5$ .

expectation value of this DO equals  $\lambda_0$  as outlined in Eq. (10), which can be estimated in the limit of large  $l$  as [51, 53]:

$$\begin{aligned}
\langle X^p \rangle &= \lambda_0 \\
&= \frac{l^2}{(2\sqrt{S} + 1)^{2l} T} \left( \sum_{i=0}^{l/2} S^i \frac{l!}{(i+1)!i!(l-2i)!} \right)^2 \\
&= \frac{l^{3/2}}{(2\sqrt{S} + 1)^{2l}} \left( \sum_{i=0}^{l/2} S^i \frac{l!}{(i+1)!i!(l-2i)!} \right)^2,
\end{aligned} \tag{60}$$

where the last line uses the relation  $T = \sqrt{l}\tilde{T} \sim \sqrt{l}$  obtained by Eq. (13) and (21). We calculate the value of the summation in the bracket numerically due to the difficulty in theoretical analysis, which is shown in Fig. 9. Based on the numerical results, we **argue** that in the large  $l$  limit  $\langle X^p \rangle \sim l^{-3/2}$ . Note that we can not exactly prove the power is strictly  $-3/2$ . Consequently, we believe the minus of logarithmic DO also exhibits logarithmic scaling expressed as:

$$-\log |\langle X^p \rangle| = \frac{3}{2} \log l + \text{const.} \tag{61}$$

We simulate this DO by MC. The results also support these findings and have been presented in Fig. 8.(b).

## VI. SUMMARY AND DISCUSSION

It has always been believed that the von Neumann entanglement entropy could be obtained through the analytic continuation of the Rényi index from Rényi entropy. However, the colored Motzkin chain serves as a counter-example, as the expression for the leading term of Rényi entanglement entropy diverges at  $n = 1$  and an extra term is needed for correction. We investigate the scaling behaviors of EE theoretically and numerically to demonstrate the failure of analytic continuation. Mathematically, this singularity is because the limits  $l \rightarrow \infty$  and

$n \rightarrow 1$  can not commute in the derivation procedures of von Neumann and Rényi entanglement entropies respectively. On the other hand, it also could be understood by the exponential increasing desity of states in its entanglement spectrum.

We have also explored the scaling of the logarithms of disorder operators under different symmetries in the colored Motzkin chains analytically and numerically. The analytic analysis predicts that all the logarithms of DOs exhibit the same scaling as Rényi EE. Our numerical simulations also confirm analytic calculations. The scaling of the von Neumann EE, Rényi EE and the logarithms of DOs point out that the coefficient of the  $\log l$  term is a universal fingerprint to the physics of Motzkin walks.

Although the entanglement entropy is difficult to measure in experiments, even in a small system [98, 99], the disorder operator is an observable that can be easily extracted particularly in cold atom platforms. We propose to probe the constrained physics of Motzkin systems intrinsically via disorder operators experimentally.

## VII. ACKNOWLEDGMENT

We thank the help of Meng Cheng on the analytical calculation. We thank the helpful discussions with Zi Hong Liu. JW and CW are supported by the National Natural Science Foundation of China under the Grant No. 12234016 and No. 12174317. ZL and ZY acknowledge the start-up funding of Westlake University, the China Postdoctoral Science Foundation under Grants No.2024M762935 and NSFC Special Fund for Theoretical Physics under Grants No.12447119. The authors thank the high-performance computing center of Westlake University and the Beijing PARATERA Tech Co.,Ltd. for providing HPC resources. This work has been supported by the New Cornerstone Science Foundation.

---

[1] L. Amico, R. Fazio, A. Osterloh, and V. Vedral, Entanglement in many-body systems, *Rev. Mod. Phys.* **80**, 517 (2008).

[2] N. Laflorencie, Quantum entanglement in condensed matter systems, *Physics Reports* **646**, 1 (2016), quantum entanglement in condensed matter systems.

[3] B. Zeng, X. Chen, D.-L. Zhou, X.-G. Wen, *et al.*, *Quantum information meets quantum matter* (Springer, 2019).

[4] M. A. Nielsen and I. L. Chuang, *Quantum computation and quantum information* (Cambridge university press, 2010).

[5] M. M. Wilde, *Quantum information theory* (Cambridge university press, 2013).

[6] A. Kitaev and J. Preskill, Topological entanglement entropy, *Phys. Rev. Lett.* **96**, 110404 (2006).

[7] M. Levin and X.-G. Wen, Detecting topological order in a ground state wave function, *Phys. Rev. Lett.* **96**, 110405 (2006).

[8] G. Vidal, J. I. Latorre, E. Rico, and A. Kitaev, Entanglement in quantum critical phenomena, *Physical Review Letters* **90**, 227902 (2003).

[9] V. E. Korepin, Universality of entropy scaling in one dimensional gapless models, *Phys. Rev. Lett.* **92**, 096402

(2004).

[10] Z. Wang, Z. Deng, Z. Wang, Y.-M. Ding, W. Guo, and Z. Yan, Probing phase transition and underlying symmetry breaking via entanglement entropy scanning, arXiv preprint arXiv:2409.09942 (2024).

[11] P. Calabrese and A. Lefevre, Entanglement spectrum in one-dimensional systems, *Phys. Rev. A* **78**, 032329 (2008).

[12] E. Fradkin and J. E. Moore, Entanglement entropy of 2d conformal quantum critical points: Hearing the shape of a quantum drum, *Phys. Rev. Lett.* **97**, 050404 (2006).

[13] Z. Nussinov and G. Ortiz, Sufficient symmetry conditions for topological quantum order, *Proc. Nat. Acad. Sci.* **106**, 16944 (2009).

[14] Z. Nussinov and G. Ortiz, A symmetry principle for topological quantum order, *Annals Phys.* **324**, 977 (2009).

[15] H. Casini and M. Huerta, Universal terms for the entanglement entropy in 2+1 dimensions, *Nucl. Phys. B* **764**, 183 (2007), arXiv:hep-th/0606256.

[16] W. Ji and X.-G. Wen, Noninvertible anomalies and mapping-class-group transformation of anomalous partition functions, *Phys. Rev. Research* **1**, 033054 (2019).

[17] W. Ji and X.-G. Wen, Categorical symmetry and noninvertible anomaly in symmetry-breaking and topological phase transitions, *Phys. Rev. Research* **2**, 033417 (2020).

[18] L. Kong, T. Lan, X.-G. Wen, Z.-H. Zhang, and H. Zheng, Algebraic higher symmetry and categorical symmetry: A holographic and entanglement view of symmetry, *Phys. Rev. Research* **2**, 043086 (2020).

[19] X.-C. Wu, W. Ji, and C. Xu, Categorical symmetries at criticality, *Journal of Statistical Mechanics: Theory and Experiment* **2021**, 073101 (2021).

[20] W. Ding, N. E. Bonesteel, and K. Yang, Block entanglement entropy of ground states with long-range magnetic order, *Physical Review A* **77**, 052109 (2008).

[21] Q.-C. Tang and W. Zhu, Critical scaling behaviors of entanglement spectra, *Chinese Physics Letters* **37**, 010301 (2020).

[22] J. Zhao, Z. Yan, M. Cheng, and Z. Y. Meng, Higher-form symmetry breaking at ising transitions, *Phys. Rev. Research* **3**, 033024 (2021).

[23] X.-C. Wu, C.-M. Jian, and C. Xu, Universal features of higher-form symmetries at phase transitions, *SciPost Phys.* **11**, 33 (2021).

[24] J. Zhao, Y.-C. Wang, Z. Yan, M. Cheng, and Z. Y. Meng, Scaling of entanglement entropy at deconfined quantum criticality, *Physical Review Letters* **128**, 010601 (2022).

[25] B.-B. Chen, H.-H. Tu, Z. Y. Meng, and M. Cheng, Topological disorder parameter: A many-body invariant to characterize gapped quantum phases, *Phys. Rev. B* **106**, 094415 (2022).

[26] J. Zhao, B.-B. Chen, Y.-C. Wang, Z. Yan, M. Cheng, and Z. Y. Meng, Measuring rényi entanglement entropy with high efficiency and precision in quantum monte carlo simulations, *npj Quantum Materials* **7**, 69 (2022).

[27] Z. Yan and Z. Y. Meng, Unlocking the general relationship between energy and entanglement spectra via the wormhole effect, *Nature Communications* **14**, 2360 (2023).

[28] P. Calabrese and J. Cardy, Entanglement entropy and quantum field theory, *Journal of Statistical Mechanics: Theory and Experiment* **2004**, P06002 (2004).

[29] Y.-M. Ding, Y. Tang, Z. Wang, Z. Wang, B.-B. Mao, and Z. Yan, Tracking the variation of entanglement rényi negativity: an efficient quantum monte carlo method (2024), arXiv:2409.10273 [cond-mat.str-el].

[30] Y.-M. Ding, J.-S. Sun, N. Ma, G. Pan, C. Cheng, and Z. Yan, Reweight-annealing method for calculating the value of partition function via quantum monte carlo (2024), arXiv:2403.08642 [cond-mat.stat-mech].

[31] M. A. Metlitski and T. Grover, Entanglement entropy of systems with spontaneously broken continuous symmetry, arXiv e-prints , arXiv:1112.5166 (2011), arXiv:1112.5166 [cond-mat.str-el].

[32] Z. Deng, L. Liu, W. Guo, and H. Lin, Improved scaling of the entanglement entropy of quantum antiferromagnetic heisenberg systems, *Physical Review B* **108**, 125144 (2023).

[33] Z. Deng, L. Liu, W. Guo, and H.-q. Lin, Diagnosing  $so(5)$  symmetry and first-order transition in the  $j - q_3$  model via entanglement entropy, arXiv preprint arXiv:2401.12838 (2024).

[34] Z. Wang, Z. Wang, Y.-M. Ding, B.-B. Mao, and Z. Yan, Bipartite reweight-annealing algorithm to extract large-scale data of entanglement entropy and its derivative in high precision (2024), arXiv:2406.05324 [cond-mat.str-el].

[35] T. Grover, Y. Zhang, and A. Vishwanath, Entanglement entropy as a portal to the physics of quantum spin liquids, *New Journal of Physics* **15**, 025002 (2013).

[36] M. Nozaki, T. Numasawa, and T. Takayanagi, Quantum entanglement of local operators in conformal field theories, *Physical review letters* **112**, 111602 (2014).

[37] J. Cardy and E. Tonni, Entanglement hamiltonians in two-dimensional conformal field theory, *Journal of Statistical Mechanics: Theory and Experiment* **2016**, 123103 (2016).

[38] P. Bueno, R. C. Myers, and W. Witczak-Krempa, Universality of corner entanglement in conformal field theories, *Physical review letters* **115**, 021602 (2015).

[39] H. Casini and M. Huerta, Positivity, entanglement entropy, and minimal surfaces, *Journal of High Energy Physics* **2012**, 87 (2012).

[40] R. Longo and F. Xu, Von neumann entropy in qft, *Communications in Mathematical Physics* **381**, 1031 (2021).

[41] P. Boes, J. Eisert, R. Gallego, M. P. Müller, and H. Wilmig, Von neumann entropy from unitarity, *Physical review letters* **122**, 210402 (2019).

[42] F. Giraldi and P. Grigolini, Quantum entanglement and entropy, *Physical Review A* **64**, 032310 (2001).

[43] W. Donnelly, Decomposition of entanglement entropy in lattice gauge theory, *Physical Review D—Particles, Fields, Gravitation, and Cosmology* **85**, 085004 (2012).

[44] T. Cubitt, A. W. Harrow, D. Leung, A. Montanaro, and A. Winter, Counterexamples to additivity of minimum output p-renyi entropy for p close to 0, *Communications in mathematical physics* **284**, 281 (2008).

[45] G. Camilo, G. T. Landi, and S. Eliëns, Strong subadditivity of the rényi entropies for bosonic and fermionic gaussian states, *Phys. Rev. B* **99**, 045155 (2019).

[46] B. Collins and I. Nechita, Random quantum channels ii: Entanglement of random subspaces, rényi entropy estimates and additivity problems, *Advances in Mathematics* **226**, 1181 (2011).

[47] E. D'Hoker, X. Dong, and C.-H. Wu, An alternative method for extracting the von neumann entropy from

rényi entropies, *Journal of High Energy Physics* **2021**, 1 (2021).

[48] J. Fuentes and J. Gonçalves, Rényi entropy in statistical mechanics, *Entropy* **24**, 1080 (2022).

[49] J. Eisert, M. Cramer, and M. B. Plenio, *Colloquium : Area laws for the entanglement entropy*, *Reviews of Modern Physics* **82**, 277 (2010).

[50] S. T. Flammia, A. Hamma, T. L. Hughes, and X.-G. Wen, Topological Entanglement Rényi Entropy and Reduced Density Matrix Structure, *Physical Review Letters* **103**, 261601 (2009).

[51] R. Movassagh and P. W. Shor, Supercritical entanglement in local systems: Counterexample to the area law for quantum matter, *Proceedings of the National Academy of Sciences* **113**, 13278 (2016), <https://www.pnas.org/doi/pdf/10.1073/pnas.1605716113>.

[52] F. Sugino and V. Korepin, Rényi entropy of highly entangled spin chains, *Int. J. Mod. Phys. B* **32**, 1850306 (2018), arXiv:1806.04049 [hep-th].

[53] V. Menon, A. Gu, and R. Movassagh, Symmetries, correlation functions, and entanglement of general quantum motzkin spin-chains, *ArXiv e-prints* (2024), arXiv:2408.16070 [quant-ph].

[54] X.-C. Wu, C.-M. Jian, and C. Xu, Universal features of higher-form symmetries at phase transitions, *SciPost Phys.* **11**, 033 (2021).

[55] E. Lake, Higher-form symmetries and spontaneous symmetry breaking, arXiv:1802.07747.

[56] E. Fradkin, Disorder operators and their descendants, *J. Stat. Phys.* **167**, 427 (2017).

[57] Z. Liu, R.-Z. Huang, Y.-C. Wang, Z. Yan, and D.-X. Yao, Measuring the boundary gapless state and criticality via disorder operator, *Phys. Rev. Lett.* **132**, 206502 (2024).

[58] J. Zhao, Z. Yan, M. Cheng, and Z. Y. Meng, Higher-form symmetry breaking at ising transitions, *Phys. Rev. Res.* **3**, 033024 (2021).

[59] Y.-C. Wang, M. Cheng, and Z. Y. Meng, Scaling of the disorder operator at  $(2+1)d$  u(1) quantum criticality, *Phys. Rev. B* **104**, L081109 (2021).

[60] Y.-C. Wang, N. Ma, M. Cheng, and Z. Y. Meng, Scaling of the disorder operator at deconfined quantum criticality, *SciPost Phys.* **13**, 123 (2022).

[61] W. Jiang, B.-B. Chen, Z. H. Liu, J. Rong, F. F. Assaad, M. Cheng, K. Sun, and Z. Y. Meng, Many versus one: The disorder operator and entanglement entropy in fermionic quantum matter, *SciPost Phys.* **15**, 082 (2023).

[62] Z. H. Liu, W. Jiang, B.-B. Chen, J. Rong, M. Cheng, K. Sun, Z. Y. Meng, and F. F. Assaad, Fermion disorder operator at gross-neveu and deconfined quantum criticalities, *Phys. Rev. Lett.* **130**, 266501 (2023).

[63] Z. H. Liu, Y. Da Liao, G. Pan, M. Song, J. Zhao, W. Jiang, C.-M. Jian, Y.-Z. You, F. F. Assaad, Z. Y. Meng, and C. Xu, Disorder operator and rényi entanglement entropy of symmetric mass generation, *Phys. Rev. Lett.* **132**, 156503 (2024).

[64] Th. Motzkin, Relations between hypersurface cross ratios, and a combinatorial formula for partitions of a polygon, for permanent preponderance, and for non-associative products, *Bulletin of the American Mathematical Society* **54**, 352 (1948).

[65] R. Donaghey and L. W. Shapiro, Motzkin numbers, *Journal of Combinatorial Theory, Series A* **23**, 291 (1977).

[66] S. Bravyi, L. Caha, R. Movassagh, D. Nagaj, and P. W. Shor, Criticality without frustration for quantum spin-1 chains, *Physical Review Letters* **109**, 207202 (2012).

[67] M. B. Hastings, I. González, A. B. Kallin, and R. G. Melko, Measuring renyi entanglement entropy in quantum monte carlo simulations, *Physical Review Letters* **104**, 157201 (2010), arXiv:1001.2335 [cond-mat.str-el].

[68] S. Humeniuk and T. Roscilde, Quantum monte carlo calculation of entanglement rényi entropies for generic quantum systems, *Physical Review B* **86**, 235116 (2012), arXiv:1203.5752 [cond-mat.str-el].

[69] S. Inglis and R. G. Melko, Wang-landau method for calculating rényi entropies in finite-temperature quantum monte carlo simulations, *Physical Review E* **87**, 013306 (2013).

[70] P. Broecker and S. Trebst, Rényi entropies of interacting fermions from determinantal quantum monte carlo simulations, *Journal of Statistical Mechanics: Theory and Experiment* **2014**, P08015 (2014).

[71] D. J. Luitz, X. Plat, N. Laflorencie, and F. Alet, Improving entanglement and thermodynamic rényi entropy measurements in quantum monte carlo, *Physical Review B* **90**, 125105 (2014).

[72] J. Pei, S. Han, H. Liao, and T. Li, The rényi entanglement entropy of a general quantum dimer model at the RK point: A highly efficient algorithm, *Journal of Physics: Condensed Matter* **26**, 035601 (2014).

[73] L. Wang and M. Troyer, Renyi entanglement entropy of interacting fermions calculated using the continuous-time quantum monte carlo method, *Physical Review Letters* **113**, 110401 (2014).

[74] F. F. Assaad, Stable quantum monte carlo simulations for entanglement spectra of interacting fermions, *Physical Review B* **91**, 125146 (2015).

[75] J. D'Emidio, Entanglement entropy from nonequilibrium work, *Physical Review Letters* **124**, 110602 (2020), arXiv:1904.05918 [cond-mat.str-el].

[76] J. Zhao, B.-B. Chen, Y.-C. Wang, Z. Yan, M. Cheng, and Z. Y. Meng, Measuring rényi entanglement entropy with high efficiency and precision in quantum monte carlo simulations, *npj Quantum Materials* **7**, 69 (2022), arXiv:2112.15178 [cond-mat.str-el].

[77] Z. Yan and Z. Y. Meng, Unlocking the general relationship between energy and entanglement spectra via the wormhole effect, *Nature Communications* **14**, 2360 (2023), arXiv:2112.05886 [cond-mat.str-el].

[78] X. Zhou, Z. Y. Meng, Y. Qi, and Y. Da Liao, Incremental SWAP operator for entanglement entropy: Application for exponential observables in quantum monte carlo simulation, *Phys. Rev. B* **109**, 165106 (2024), arXiv:2401.07244 [cond-mat.str-el].

[79] Z. Yan and Z. Y. Meng, Unlocking the general relationship between energy and entanglement spectra via the wormhole effect, *Nature Communications* **14**, 2360 (2023).

[80] Z. Liu, R.-Z. Huang, Z. Yan, and D.-X. Yao, Demonstrating the wormhole mechanism of the entanglement spectrum via a perturbed boundary, *Physical Review B* **109**, 094416 (2024).

[81] C. Li, R.-Z. Huang, Y.-M. Ding, Z. Y. Meng, Y.-C. Wang, and Z. Yan, Relevant long-range interaction of the entanglement hamiltonian emerges from a short-range gapped system, *Physical Review B* **109**, 195169 (2024).

[82] L. P. Kadanoff and H. Ceva, Determination of an operator algebra for the two-dimensional ising model, *Physical Review B* **3**, 3918 (1971).

[83] F. J. Wegner, Duality in Generalized Ising Models and Phase Transitions without Local Order Parameters, *Journal of Mathematical Physics* **12**, 2259 (1971).

[84] E. Fradkin and L. Susskind, Order and disorder in gauge systems and magnets, *Physical Review D* **17**, 2637 (1978).

[85] Z. Nussinov and G. Ortiz, A symmetry principle for topological quantum order, *Annals of Physics* **324**, 977 (2009).

[86] A. Kapustin and N. Seiberg, Coupling a QFT to a TQFT and duality, *Journal of High Energy Physics* **2014**, 1 (2014).

[87] D. Gaiotto, A. Kapustin, N. Seiberg, and B. Willett, Generalized global symmetries, *Journal of High Energy Physics* **2015**, 172 (2015).

[88] E. Fradkin, Disorder operators and their descendants, *Journal of Statistical Physics* **167**, 427 (2017), arXiv:1610.05780 [cond-mat.stat-mech].

[89] X.-G. Wen, *Colloquium* : Zoo of quantum-topological phases of matter, *Reviews of Modern Physics* **89**, 041004 (2017).

[90] X.-G. Wen, Choreographed entanglement dances: Topological states of quantum matter, *Science* **363**, eaal3099 (2019).

[91] W. Ji and X.-G. Wen, Categorical symmetry and noninvertible anomaly in symmetry-breaking and topological phase transitions, *Physical Review Research* **2**, 033417 (2020), arXiv:1912.13492 [cond-mat.str-el].

[92] W. Witczak-Krempa, Entanglement susceptibilities and universal geometric entanglement entropy, *Phys. Rev. B* **99**, 075138 (2019), arXiv:1810.07209 [cond-mat.str-el].

[93] L. Kong, T. Lan, X.-G. Wen, Z.-H. Zhang, and H. Zheng, Algebraic higher symmetry and categorical symmetry: A holographic and entanglement view of symmetry, *Physical Review Research* **2**, 043086 (2020).

[94] X.-C. Wu, W. Ji, and C. Xu, Categorical symmetries at criticality, *Journal of Statistical Mechanics: Theory and Experiment* **2021**, 073101 (2021), arXiv:2012.03976 [cond-mat.str-el].

[95] J. Zhao, Z. Yan, M. Cheng, and Z. Y. Meng, Higher-form symmetry breaking at ising transitions, *Physical Review Research* **3**, 033024 (2021), arXiv:2011.12543 [cond-mat.str-el].

[96] Y.-C. Wang, M. Cheng, and Z. Y. Meng, Scaling of disorder operator at  $\mathbb{S}(2+1)d\mathbb{S} U(1)$  quantum criticality, *Physical Review B* **104**, 081109 (2021), arXiv:2101.10358 [cond-mat.str-el].

[97] W. Jiang, B.-B. Chen, Z. H. Liu, J. Rong, F. F. Asaad, M. Cheng, K. Sun, and Z. Y. Meng, Many versus one: The disorder operator and entanglement entropy in fermionic quantum matter, *SciPost Phys.* **15**, 082 (2023), arXiv:2209.07103 [cond-mat.str-el].

[98] R. Islam, R. Ma, P. M. Preiss, M. Eric Tai, A. Lukin, M. Rispoli, and M. Greiner, Measuring entanglement entropy in a quantum many-body system, *Nature* **528**, 77 (2015).

[99] D. A. Abanin and E. Demler, Measuring entanglement entropy of a generic many-body system with a quantum switch, *Phys. Rev. Lett.* **109**, 020504 (2012).